CILAMCE
PANACM
RIO DE JANEIRO 2021

A numerical study of damage evaluation in jointed plain concrete pavements considering alternative materials for dowel bars

Edmir J. Santos Júnior, Sérgio G.F. Cordeiro, Francisco A. C. Monteiro

Laboratório de Modelagem Estrutural – LME, Instituto Tecnológico de Aeronáutica.
Praça Marechal Eduardo Gomes, 50, Vila das Acácias, 12.228-900, São José dos Campos/SP, Brasil
edmir.junior@ga.ita.br, cordeiro@ita.br, facm@ita.br

Abstract. It is well-known in the design of jointed plain concrete pavements (JPCP) that the concrete damage due to stress near the dowel bars is a key factor that affects the service life of such structures. This study aimed to evaluate numerically the differences in the damage distribution in the concrete near the dowel bars in JPCP considering alternative materials for the bars. Two materials were considered for the dowels: steel and glass fiber reinforced polymer (GFRP). The adopted constitutive model for the concrete was the concrete damage plasticity. Interactions between the concrete and the dowel bars were simulated by surface-to-surface contact type. The finite element models were validated by comparing available experimental load-displacement curves with the obtained numerical ones. The results for the damage distributions reveal that the use of GFRP bars has induced smaller damage values within a smaller damaged zone when compared with the dowel steel bar model. As a consequence, smaller cracks in such zones will appear which will increase the structural life of the pavement. Also, a higher ultimate load for JPCP with GFRP bars is observed.

Keywords: jointed plain concrete pavement, glass fiber reinforced polymer dowel bar, concrete damage plasticity, numerical damage evaluation.

1 Introduction

The jointed plain concrete pavement (JPCP) consists of concrete slabs separated by joints and rested on one or more foundation layers. The existence of joints in this type of pavement is associated with three main factors: construction, shrinkage and expansion. Construction joints (Fig. 1a) stand between slabs and occur when concrete is poured over already existing concrete; shrinkage joints control the random cracking process of concrete and expansion joints separate structures subject to movement in different directions [1]. The long-term performance of JPCP is directly related to the load transfer efficiency at the joints. The aggregate interlock is a natural load transfer device and consists of the mechanical closure formed in the joints. In the construction joints, this mechanism is absent, making the use of dowel bars mandatory as a load transfer device between slabs [2]. The load transfer through the dowel bars occurs by transversal shear and/or bending moment. This mechanism generates a stress concentration in the vicinity of the bars (Fig. 1b), making it a critical zone for microcracking. This degradation impacts the performance and service life of such structures [3]. Researchers have been testing alternative geometric design, as well as alternative materials for dowel bars, in order to reduce the stress concentration. Wakdar et. al. [4] evaluated the influence of dowel diameter, spacing, and length parameters on the load transfer efficiency in joints. Kim and Hjelmstad [5] and Mackiewicz [3] analyzed the dowel looseness and its implication on the stress state on the concrete in the vicinity of the dowel. Sadegui and Hesami [6] and Shoukry et. al. [7] evaluated the friction between the dowel and the concrete pavement. Prabhu et. al. [8] and Al-Humeidawi and Mandal [9] evaluated the consequences of misalignment of the dowels in relation to the level of stress around the bars. Al-Humeidawi and Mandal [10] evaluated experimentally the vertical displacement of dowel bars comparing steel bars with glass fiber reinforced polymer (GFRP) bars.

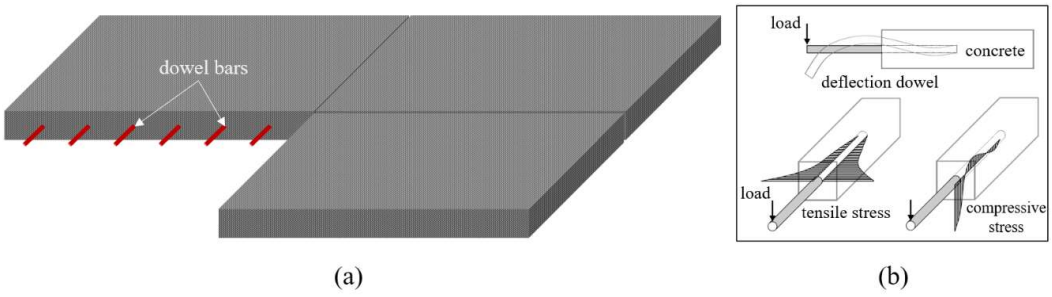

Figure 1. JPCP: (a) construction joints with dowel bars; (b) distribution of stress in a loaded dowel

In this study, a finite element model was developed in order to analyze the load transfer capacity and evaluate the damage of the concrete in the vicinity of the dowel bars for two different types of dowel bars: steel and GFRP. A representative structure of a construction joint was modeled to evaluate the dowel bars behavior through a fully nonlinear (geometrical and material) finite element analysis. The constitutive model used for the concrete was the concrete damage plasticity (CDP), which allows for the damage evaluation and it is claimed being accurate for the evaluation of the ultimate load of concrete structures. The model updating was made from experimental results by [10].

2 Concrete damage plasticity constitutive model

The concrete damage plasticity (CDP) is a continuum constitutive model of damage plasticity formulation developed by [11] and later modified by [12]. It assumes two main failure mechanisms for the concrete: tensile cracking and compression crushing. Cracks are represented macroscopically by stiffness degradation through a scalar damage variable. The yield surface is controlled by the hardening variables $\tilde{\varepsilon}_t^p$ and $\tilde{\varepsilon}_c^p$, which corresponds to the equivalent tensile and compressive plastic strains, respectively, and are related to the failure mechanisms in tensile and compression. This model is capable of accurately predicting the response of different concrete structures under different types of loading [13] – [15].

2.1 Uniaxial behavior under tension and compression

The behavior under uniaxial tension starts with a linear elastic part until it reaches the maximum tensile stress σ_{t0}, which represents the beginning of the tensile cracking. After this value, the response turns to a softening behavior with the appearance of a localized strain zone. The behavior under uniaxial compression also starts with a linear elastic range, until σ_{c0}, where compression crushing begins, follows with a strain hardening part until the ultimate stress σ_{cu} and, beyond this value, enters in the softening range. Figure 2 shows a schematic representation of the response of concrete under uniaxial stress state.

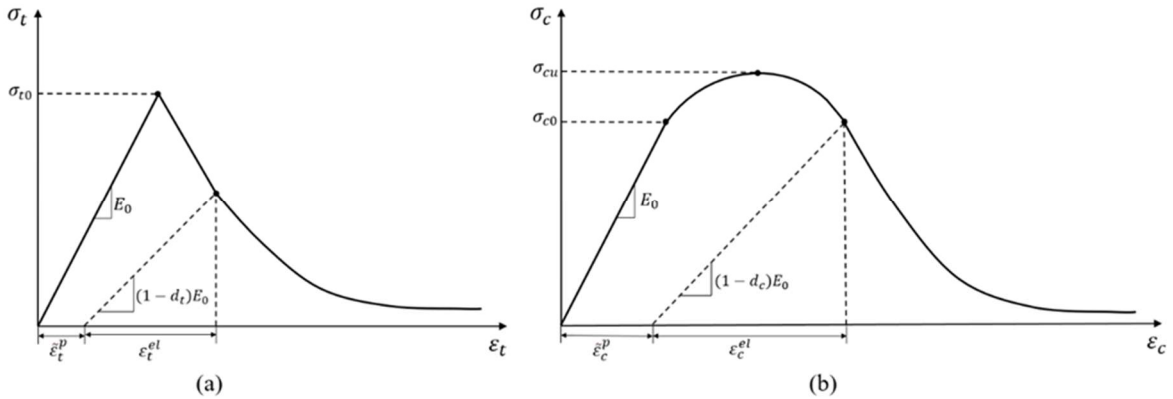

Figure 2. Uniaxial stress-strain behavior: (a) tension; (b) compression

The strains after unloading until a null stress condition, regarding stiffness degradation, are the equivalent plastic strains $\tilde{\varepsilon}_t^p$ and $\tilde{\varepsilon}_c^p$, as illustrated in Fig. 2. The uniaxial stiffness degradation is different in tension and in compression. Thus, it is represented by two damage variables, namely, d_t (tensile damage) and d_c (compressive damage), which depend on the respective plastic strain, temperature, and other field variables. In the adopted model, the evolution of these variables depends only on the plastic strains.

2.2 Cyclic uniaxial behavior

When there is a cyclic loading, and the direction of the load changes, the stiffness degradation mechanism becomes quite complex and it is necessary to consider the variables of damage due to tensile and compression together. This occurs due to what is verified in the physical behavior of the material (for example, when a crack originating from a tensile load tends to close due to the change of the load to compression). This physical phenomenon results in the concept of stiffness recovery since crack closure reverts to an increase in the elastic stiffness at that given instant. Thus, the stiffness degradation is summarized by a single scalar damage variable d, according to

$$E = (1 - d)E_0 \tag{1}$$

where d is a function of the stress state and of the tension and compression damage variables d_t and d_c

$$1 - d = (1 - s_t d_c)(1 - s_c d_t) \tag{2}$$

The quantities s_t and s_c depend on the uniaxial stress σ_{11} and are defined according to

$$s_i = 1 - w_i r(\sigma_{11}) \tag{3}$$

where $0 \leq w_i \leq 1 \ \ (i = t, c)$ and

$$r(\sigma_{11}) = \begin{cases} 1 & \sigma_{11} > 0 \\ 0 & \sigma_{11} < 0 \end{cases} \tag{4}$$

The constants w_t and w_c are responsible for controlling the elastic stiffness recovery, as the load changes sign, and are assumed to be material properties.

2.3 Damage under tensile, compression and evolution laws

Hillerborg [17] defines the fracture energy G_f as the energy required to open a unit area of crack. This is a material parameter, used in the conceptualization of brittle fracture materials. From the definition of the crack opening displacement u_t^{ck} and the tensile damage d_t, the plastic tensile displacement u_t^p is given by

$$u_t^p = u_t^{ck} - \frac{d_t}{1 - d_t}\frac{\sigma_t l_0}{E_0} \tag{5}$$

where l_0 is the characteristic length, which to overcame mesh dependency, is defined as the average size of the finite elements in the vicinity of the damaged region.

The stiffness degradation related to compression crushing occurs after the elastic regime. This behavior is defined from the compressive stress σ_c versus inelastic compressive strain ε_c^{in} data, where

$$\varepsilon_c^{in} = \varepsilon_c - \varepsilon_{0c}^{el} \tag{6}$$

in which ε_c is the total uniaxial compressive strain and $\varepsilon_{0c}^{el} = \sigma_c / E_0$ is the elastic compressive strain corresponding to the material without damage. The plastic strain is then obtained from the following relationship:

$$\varepsilon_c^p = \varepsilon_c^{in} - \frac{d_c}{1 - d_c}\frac{\sigma_c}{E_0} \tag{7}$$

The evolution laws for the damage variables d_t and d_c used in this work were obtained from experimental tests of cyclical tensile and compressive loadings by Birtel and Mark [18].

2.4 Multiaxial behavior

The CDP is an isotropic damage model. Therefore, the damage variable remains scalar in the multiaxial case and the degradation of the elastic stiffness occurs reducing equally the components of the constitutive elastic tensor $\mathbf{D_0}$. Thus, the stress-strain relationship for general multiaxial case results

$$\boldsymbol{\sigma} = (1-d)\boldsymbol{D}_0 : (\boldsymbol{\varepsilon} - \boldsymbol{\varepsilon}^p) \tag{8}$$

where $\boldsymbol{\sigma}$, $\boldsymbol{\varepsilon}$ and $\boldsymbol{\varepsilon}^p$ are, respectively, the stress, total strain and plastic strain tensors. The scalar damage variable d is defined exactly as presented in (2). The difference in the multiaxial case occurs in the definition of the functions r, which now depends on the stress tensor $\boldsymbol{\sigma}$, as shown below

$$r(\boldsymbol{\sigma}) = \sum_{i=1,3} \langle \sigma_i \rangle \Big/ \sum_{i=1,3} |\sigma_i| \qquad \langle \sigma_i \rangle = \frac{1}{2}(\sigma_i + |\sigma_i|) \tag{9}$$

in which σ_i $(\sigma_1 \geq \sigma_2 \geq \sigma_3)$ are the principal stresses of $\boldsymbol{\sigma}$. From (8), the concept of effective stress tensor $\overline{\boldsymbol{\sigma}}$ can be established as

$$\overline{\boldsymbol{\sigma}} = \boldsymbol{D}_0 : (\boldsymbol{\varepsilon} - \boldsymbol{\varepsilon}^p) \qquad \overline{\boldsymbol{\sigma}} = \frac{\boldsymbol{\sigma}}{(1-d)}. \tag{10}$$

2.5 Concrete plasticity

The CDP is a plasticity model coupled with isotropic damage. Thus, the yielding surface adopted by Lubliner et. al. [11] is defined in terms of the invariants of the effective stress tensor $\overline{\boldsymbol{\sigma}}$ as

$$F(\bar{\sigma}_1, \bar{p}, \bar{q}) = \frac{1}{1-\alpha}\left(\bar{q} - 3\alpha\bar{p} + \beta\left(\tilde{\varepsilon}_c^p, \tilde{\varepsilon}_t^p\right)\langle\bar{\sigma}_1\rangle - \gamma\langle -\bar{\sigma}_1\rangle\right) - \bar{\sigma}_c\left(\tilde{\varepsilon}_c^p\right) = 0 \tag{11}$$

where $\bar{\sigma}_1$ is the maximum principal effective stress and $\bar{p}$, $\bar{q}$ are, respectively, the hydrostatic pressure effective stress and the Von Misses effective stress

$$\bar{p} = -\frac{1}{3}tr(\overline{\boldsymbol{\sigma}}) \qquad \bar{q} = \sqrt{\frac{3}{2}(\overline{\boldsymbol{S}} : \overline{\boldsymbol{S}})} \qquad \overline{\boldsymbol{S}} = \overline{\boldsymbol{\sigma}} + \bar{p}\boldsymbol{I}. \tag{12}$$

The uniaxial compressive effective stress $\bar{\sigma}_c\left(\tilde{\varepsilon}_c^p\right)$ and $\beta\left(\tilde{\varepsilon}_c^p, \tilde{\varepsilon}_t^p\right)$ are hardening variables, controlled by $\tilde{\varepsilon}_c^p$, $\tilde{\varepsilon}_t^p$, and α, γ are material parameters. Let $\delta = \sigma_{b0}/\sigma_{c0}$ be the ratio between the initial equibiaxial compressive yield stress σ_{b0} and the initial uniaxial compressive yield stress σ_{c0}, then

$$\alpha = \frac{\delta - 1}{2\delta - 1}. \tag{13}$$

Regarding the uniaxial tensile $\bar{\sigma}_t(\tilde{\varepsilon}_t^p)$ and compressive $\bar{\sigma}_c(\tilde{\varepsilon}_c^p)$ effective stresses, one defines

$$\beta\left(\tilde{\varepsilon}_c^p, \tilde{\varepsilon}_t^p\right) = \frac{\bar{\sigma}_c(\tilde{\varepsilon}_c^p)}{\bar{\sigma}_t(\tilde{\varepsilon}_t^p)}(1-\alpha) - (1+\alpha). \tag{14}$$

The last material parameter reads

$$\gamma = \frac{3(1-K_c)}{2K_c - 1} \tag{15}$$

where K_c is the ratio between the Von Misses stress on the tensile meridian of the yield surface $q(\mathrm{TM})$, to that on the compressive meridian $q(\mathrm{CM})$, at initial yield for any given value of the hydrostatic pressure p such that the maximum principal stress is negative $(\sigma_1 < 0)$.

The CDP assumes a non-associated potential plastic flow. The flow potential G used in this model is the Drucker-Prager hyperbolic function

$$G = \sqrt{(\epsilon\sigma_{t0}tan\Psi)^2 + \bar{q}^2} - \bar{p}tan\Psi \tag{16}$$

where Ψ is the dilation angle measured in the $\bar{q} \times \bar{p}$ plane for high values of $\bar{p}$, σ_{t0} is the uniaxial tensile stress at failure and ϵ is an eccentricity parameter, which defines the rate at which the function approaches the asymptote.

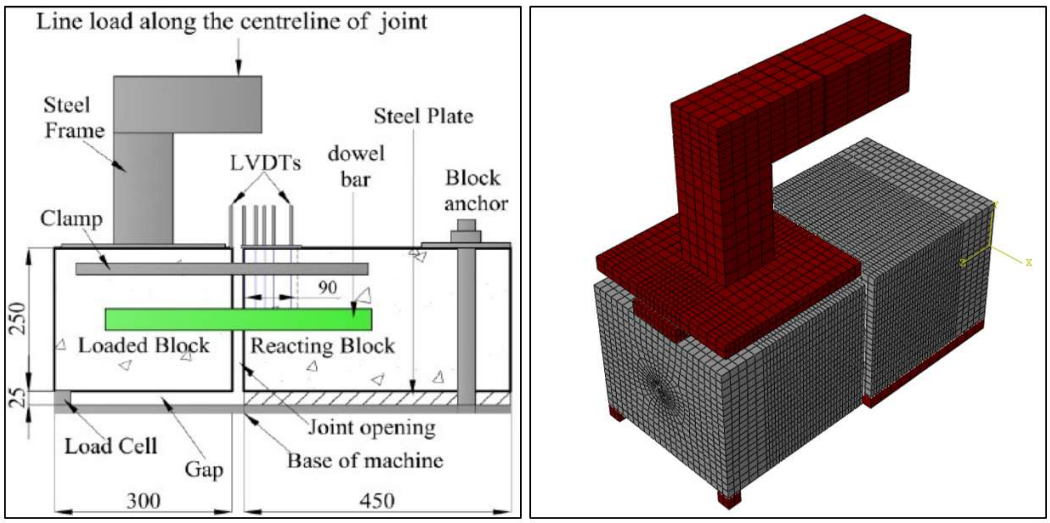

Figure 3. Representative structure: (a) component parts; (b) finite element model

3 Finite element model results

The developed finite element model is a structure representative of a rigid pavement construction joint, which was proposed on the laboratory tested performed by Al-Humeidawi and Mandal [10]. The validation of the model was based on their experimental results, presented in terms of the displacements of the upper face of the dowel bar at the face of the reacting block. Figure 3 presents a scheme of the structure tested by Al-Humeidawi and Mandal [10] and the developed finite element model. A compressive strength (concrete cube test) of 30 MPa was considered in both experimental and numerical tests. The compressive stress-strain curve (Fig. 4a) and the tensile stress crack opening displacement curve (Fig. 4b) were obtained from Al-Humeidawi [19]. Others conventional concrete parameters were obtained by standard codes BS EN 1992-1-1 [20] and CEB-FIP 1990 [21]. The adopted yielding surface and flow potential parameters were $\delta = 1.16$, $K_c = 0.67$, $\epsilon = 0.1$ and $\Psi = 30°$ [19]. The concrete viscosity adopted was 3×10^{-4}, based in values for viscosity parameter reported by literature to attain convergence in models [22].

The steel used in the dowel bar, and in different parts of the model, is an elastoplastic material following the Von Mises plasticity model with linear hardening. The material constants adopted for the steel were the same as in Al-Humeidawi and Mandal [10]: density of $7780\ \mathrm{kg/m^3}$, elastic constants $E = 200$ GPa and $\nu = 0.3$, yield stress of 275 MPa and ultimate stress of 460 MPa. The GFRP used in the dowel bar as an alternative to the steel bar is a transversely isotropic material with respect to the xy material plane, which is aligned with the XY global plane. This material has a density of $1900\ \mathrm{kg/m^3}$ and elastic constants $E_x = E_y = 10$ GPa,$E_z = 40.8$ GPa, $\nu_{12} = 0.22$, $\nu_{12} = 0.071$ and $G_{xz} = G_{yz} = 3.62$ GPa [10].

A surface-to-surface contact type simulates the connection between the dowel bar and the concrete blocks. The adopted friction coefficients are 0.05 (loaded block) and 0.35 (reacting block) for the model with steel the dowel bar. In the model with the GFRP bar, the adopted friction is 0.016 on both blocks. Such values have been proposed by Al-Humeidawi [19]. The other contacts between the structural components are of the constraint type. Regarding the geometric boundary conditions, the reacting block is fixed on its base, while both blocks are prevented from lateral movement. The loaded block is frictionless supported on load cells. According to Fig. 3a, a line loading type is applied at the steel frame along the centerline of the joint. All component parts are modeled with the solid C3D8R element, resulting in a total of 89908 elements for the steel dowel bar model, and 85456 for the GFRP dowel bar model.

The validation of the models was made taking the displacement experimental data of the upper surface of the bar at the face of the reacting block, available in Al-Humeidawi and Mandal [10]. Figure 5 shows the comparison between the experimental results and the developed models. The damage distributions in the concrete around the dowel bar at both the loaded and the reacting blocks was obtained with the numerical models.

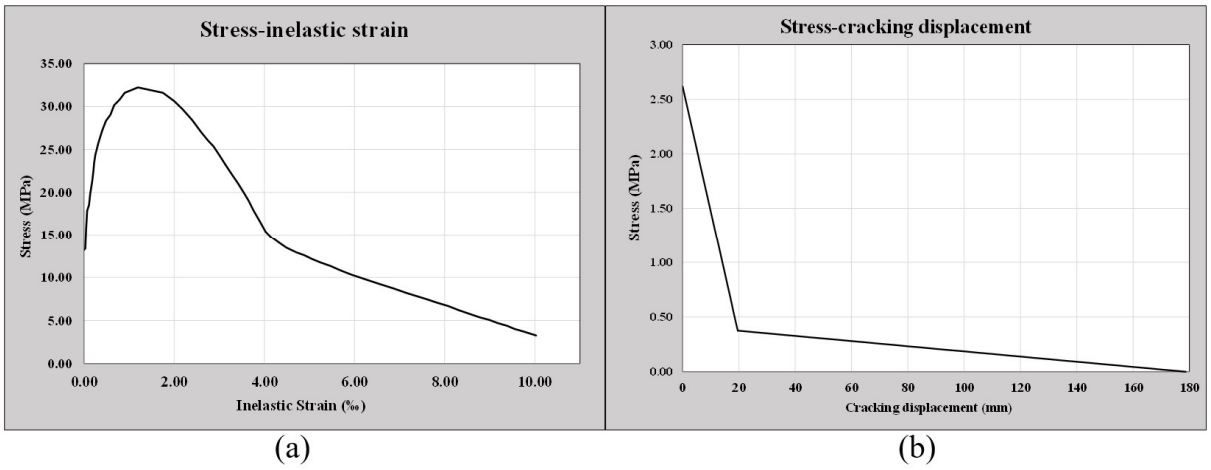

Figure 4. Inelastic behavior of concrete: (a) compression; (b) tension

Figure 6 compares the damage distributions of the model with the steel bar and the model with the GFRP bar for an applied load of 40 kN. It can be observed that there is a smaller damaged region in the GFRP bar model compared with the steel model. The lower stiffness of the GFRP, in comparison with the steel, is the main factor for the difference in the damage distribution of these models. It is noteworthy that the greater the damaged region, the greater the possibility of microcracking and, consequently, the reduction of the structure's service life. Another important difference between the two models is the ultimate load supported by each of them: while the ultimate load for the steel bar model was 42 kN, the ultimate load for the GFRP bar model was 62 kN. The grey scale is the same for all results shown: black for maximum damage ($d = 1$) and white for minimum damage ($d = 0$).

4 Conclusions

This paper evaluated numerically the differences in the damage distribution in the concrete near the dowel bars in JPCP considering alternative materials for the dowel bars. A finite element model was developed using Abaqus and validated from the available experimental results of displacement of the bar at the face of the joint. Two different materials were analyzed for the dowel bar: steel and GFRP, a transversely isotropic material, alternative to steel. The constitutive model used for the concrete was the CDP and the scalar damage variable distribution was evaluated in both structures. After the validation of the model, the damage values and its distributions around the dowel bar in each model was compared.

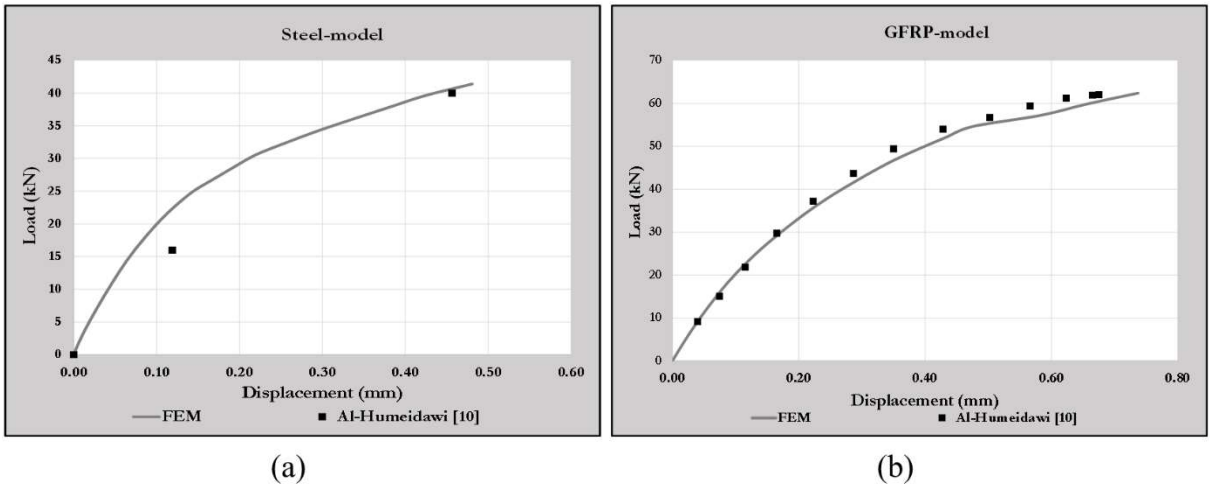

Figure 5. Experimental and numerical results: (a) steel bar model; (b) GFRP bar model.

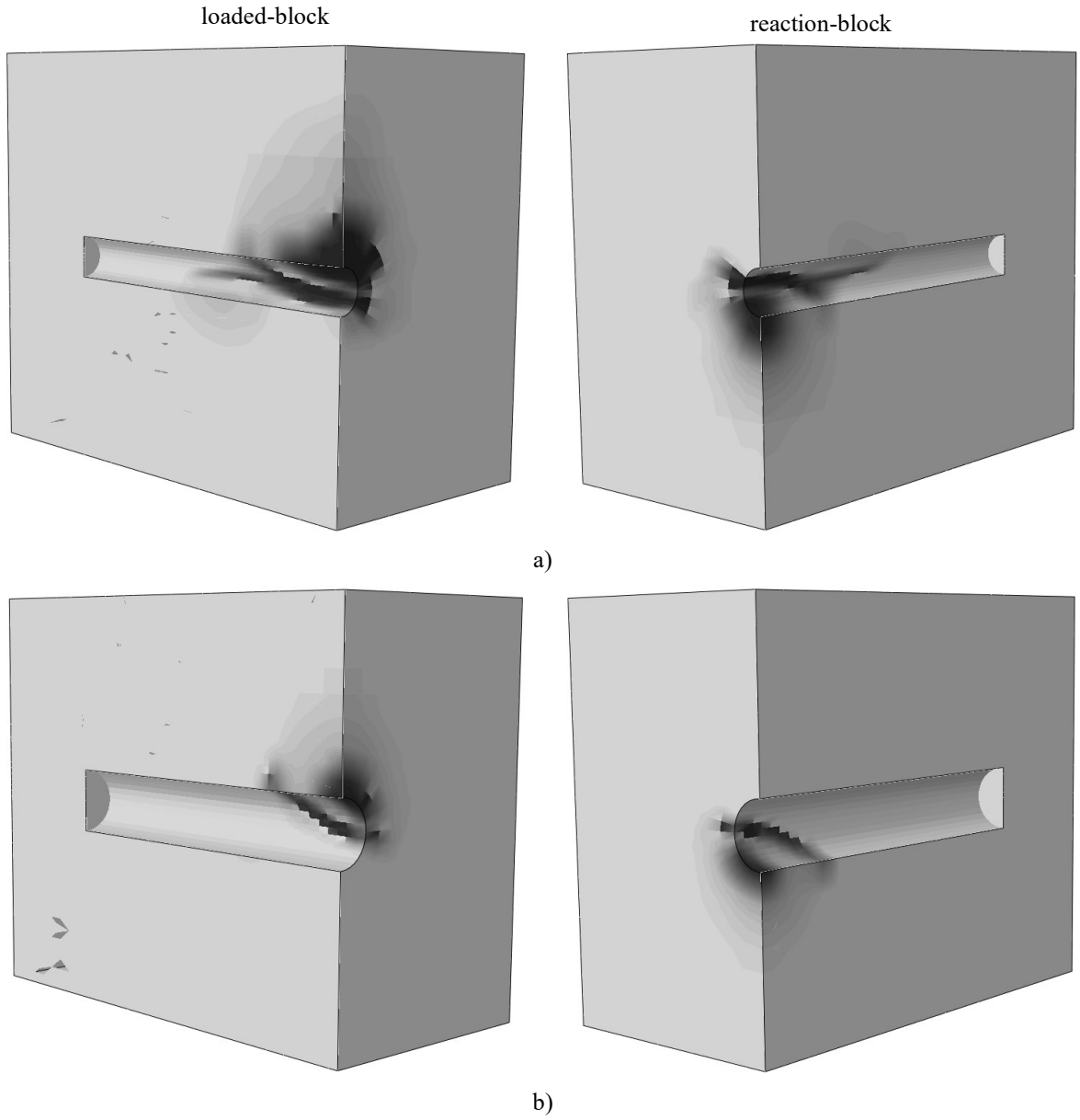

Figure 6. Comparison of the scalar damage variable distributions: (a) steel bar model; (b) GFRP bar model

A greater damaged region was observed in the steel bar model, for the same load level, when compared with the GFRP bar model. This greater damaged region generates a higher potential for cracking, directly affecting the service life of the structure. Finally, it was also observed that the ultimate load of the GFRP bar model was greater than the steel bar model, indicating another possible advantage of using such alternative material.

Authorship statement. The authors hereby confirm that they are the sole liable persons responsible for the authorship of this work, and that all material that has been herein included as part of the present paper is either the property (and authorship) of the authors or has the permission of the owners to be included here.

References

[1] E. J. Yoder and M. W. Witczak. *Principles of pavement design*. John Wiley & Sons, 1991.

[2] Y. H. Huang. *Pavement analysis and design*. Prentice-Hall, 1993.

[3] P. Mackiewicz. "Finite-element analysis of stress concentration around dowel bars in jointed plain concrete pavement". *Journal of Transportation Engineering*, vol. 141, n. 6, pp. 06015001 (1–8), 2015.

[4] A. Wadkar, Y. Metha, D. Cleary, A. Zapata, L. Musumeci and K. William. "Effect of aircraft gear positions and gear configurations on load transfer efficiency of airfield rigid pavement joints". *Road Pavement and Material Characterization, Modeling, and Maintenance*. pp. 40–48, 2011.

[5] J. Kim and K. D. Hjelmstad. "Three-dimensional finite element analysis of doweled joints for airport pavements". *Transportation Research Record*, vol. 1853, n. 1, pp. 100–109, 2003.

[6] V. Sadeghi and S. Hesami. "Investigation of load transfer efficiency in jointed plain concrete pavements (JPCP) using FEM". *International Journal of Pavement Research and Technology*, vol. 11, n. 3, pp. 245–252, 2018.

[7] S. N. Shoukry, G. W. William, M. Y. Riad and S. V. S. Motamarri. Effect of Bonding Force on Stresses in Concrete Slabs. PhD thesis, West Virginia University, College of Engineering and Mineral Resources, 2003.

[8] M. Prabhu, A. Varma and N. Buch. "Analytical investigation of the effects of dowel misalignment on concrete pavement joint opening behaviour". *International Journal of Pavement Engineering*, vol. 10, n. 1, pp. 49–62, 2009.

[9] B. H. Al-Humeidawi and P. Mandal. "Experimental investigation on the combined effect of dowel misalignment and cyclic wheel loading on dowel bar performance in JPCP". *Engineering Structures*, vol. 174, pp. 256–266, 2018.

[10] B. H. Al-Humeidawi and P. Mandal. "Evaluation of performance and design of GFRP dowels in jointed plain concrete pavement–part 1: experimental investigation". *International Journal of Pavement Engineering*, vol. 15, n. 5, pp. 449–459, 2014.

[11] J. Lubliner, J. Oliver, S. Oller and E. Onate. "A plastic-damage model for concrete". *International Journal of solids and structures*, vol. 25, n. 3, pp. 299–326, 1989.

[12] J. Lee and G. L. Fenves. "Plastic-damage model for cyclic loading of concrete structures". *Journal of engineering mechanics*, vol. 124, n. 8, pp. 892–900, 1998.

[13] Y. Tao and J. Chen. "Concrete damage plasticity model for modeling FRP-to-concrete bond behavior". *Journal of composites for construction*, vol. 19, n. 1, pp. 04014026 (1–13), 2015.

[14] H. Othman and H. Marzouk. "Finite-element analysis of reinforced concrete plates subjected to repeated impact loads". *Journal of Structural Engineering*, vol. 143, n. 9, pp. 04017120 (1–16), 2017.

[15] N. F. Hany, E. G. Hantouche and M. H. Harajli. "Finite element modeling of FRP-confined concrete using modified concrete damaged plasticity". *Engineering Structures*, vol. 125, pp. 1–14, 2016.

[16] SIMULIA (2010). "Abaqus analysis user manual version 6.10." Dassaults system, headquartered in Providence, RI, USA.

[17] A. Hillerborg, M. Modéer and P. E. Petersson. "Analysis of crack formation and crack growth in concrete by means of fracture mechanics and finite elements". *Cement and concrete research*, vol. 6, n. 6, pp. 773–781, 1976.

[18] V. Birtel and P. Mark. Parameterized finite element modelling of RC beam shear failure. In: ABAQUS users' conference. 2006.

[19] B. H. Al-Humeidawi. Evaluation of the performance of GFRP dowels in jointed plain concrete pavement (JPCP) for road/airport under the combined effect of dowel misalignment and cyclic wheel load. PhD thesis. The University of Manchester (United Kingdom), 2013.

[20] BS EN 1992-1-1 (2004). "Eurocode 2: Design of concrete structures." Part 1-1: General rules and rules for buildings, British Standards Institution, London.

[21] CEB-FIP 1990 (1993). "Design of concrete structures." Thomas Telford, London.

[22] L. M. Silva, A. L. Christoforo and R. C. Carvalho. "Calibration of Concrete Damaged Plasticity Model parameters for shear walls". *Revista Matéria,* vol. 26, n. 01, 2021.